Banded Liquid–Liquid Taylor-Couette-Poiseuille Flow

Xiaoyan Zhu and R. Dennis Vigil
Dept. of Chemical Engineering, Iowa State University, Ames, IA 50011

It has been reported that several distinct flow patterns may result when two immiscible liquids undergo Taylor vortex flow in the annular gap between a fixed outer cylinder and a rotating concentric inner cylinder. One such flow pattern (banded flow) apparently arises when less dense disperse phase droplets migrate to Taylor vortex cores due to the centrifugal force associated with the rotation of the vortices. Using the hypothesis that centrifugally driven droplet migration to vortex cores competes with turbulent diffusion, a simple criterion for predicting when banded flow patterns arise shows consistency with numerical simulations and experiments.

Introduction

Taylor-Couette flow is a topic of sustained interest even though it has been systematically studied over many decades. Much of this interest can be attributed to its usefulness as a model system for fundamental studies in fluid mechanics. However, several features of Taylor-Couette and Taylor-Couette-Poiseuille flow are also attractive for various chemical processing applications, although Taylor-Couette devices are not widely deployed for these purposes. In particular, the superposition of an axial flow on the rapid radial and azimuthal mixing achievable in Taylor vortex flow can lead to a nearly perfect approximation of plug flow (Kataoka et al., 1975). In addition, under certain circumstances the shear environment in the vortex cores can be made relatively mild compared with the vortex outer layers (Desmet et al., 1997a,b; Campero and Vigil, 1997a), and this structure could be useful for applications such as growth of mammalian cell cultures (Tsao et al., 1994). Many other proposed or demonstrated uses for Taylor-Couette flow are listed in Table 1. Note that most of these involve multiphase and/or axial flow.

Despite the continually increasing number of proposed applications of multiphase Taylor-Couette-Poiseuille flow, reports concerning the hydrodynamic structures found in such systems have appeared only recently. Here we are concerned specifically with liquid–liquid Taylor-Couette flow, and most of the relevant literature can be assigned to one of the following categories: (1) studies of layered flows in Couette cells with corotating cylinders or in systems with a fixed outer cylinder and low rotation rate of the inner cylinder, and (2) studies of banded and/or emulsified flow patterns in Couette cells with fixed outer cylinders and relatively high inner cylinder rotation rates. The current understanding of the stability of radially stratified liquid–liquid flow in a Couette apparatus has been developed by several authors who have numerically or experimentally investigated interfacial waves, rigid rotation, coating films, and Taylor instabilities in each fluid layer (Schneyer and Berger, 1971; Joseph et al., 1985; Renardy and Joseph, 1985; Joseph and Preziosi, 1987; King et al., 1998; Baier and Graham, 1998, 2000; Caton et al., 2000; Charru and Hinch, 2000; Albert and Charru, 2000; Roberts et al., 2000).

Much of what is known about emulsified flows in devices with fixed outer cylinders has also been reported relatively recently (Joseph et al., 1984, 1990; Campero and Vigil, 1997b, 1999; Zhu et al., 2000). Joseph et al. (1984, 1990), using a horizontal Couette cell filled with equal volumes of various pairs of aqueous and organic fluids, discovered many new flow patterns, including layered and banded Couette flows, rollers, coarse and foamy emulsions, and phase inversions. Campero and Vigil (1997b, 1999) surveyed hydrodynamic structures and studied the effects of various parameters, including density ratio, viscosity ratio, feed composition, and azimuthal Reynolds number in liquid–liquid Taylor-Couette flow with a weak axial flow ($Re_z = 0.41 - 0.56$). At least three distinct structures were found including: (1) a translating banded structure with alternating water and organic-rich vortices at low organic-phase volume fractions or sufficiently large rota-

Correspondence concerning this article should be addressed to R. D. Vigil.

Table 1. Applications of Taylor-Couette Flow

Application	Author(s)
Plug-flow reactor	Kataoka et al. (1975)
Emulsion polymerization	Imamura et al. (1993); Kataoka et al. (1995)
Monodisperse silica-particle synthesis	Ogihara et al. (1995)
Heterogeneous catalytic reactor	Cohen and Maron (1983, 1991)
Heterogeneous photocatalytic reactor	Sczechowski et al. (1995); Miller et al. (1964)
Recovery of reaction intermediates	Vigil et al. (1992); Ouyang et al. (1992)
Liquid–liquid mixing	Haas (1987); Leonard et al. (1981)
Liquid–liquid extraction	Thornton and Pratt (1953); Davis and Weber (1960); Bernstein et al. (1973); Baier and Graham (1998, 2000)
Homogeneous reactions, particle coating	Holl (1996)
Mammalian cell culture	Tsao et al. (1994)
Blood heparin neutralization	Ameer et al. (1999)
Membrane separation/reaction	Wronski et al. (1999)
Filtration	Holeschovsky and Cooney (1991); Wereley and Lueptow (1999)
Precipitation	Jung et al. (2000)

tion rates; (2) a spatially homogeneous emulsion with phase inversion at high organic-phase volume fraction and moderate rotation rates; and (3) an axially translating periodic variation between the banded and homogeneous states at low rotation rates. Photographic evidence showed that the banded flow pattern does not consist of separate aqueous and organic-rich vortices. Instead, the banded appearance is caused by disperse-phase droplet migration to vortex cores. A series of experiments with various fluid pairs suggested that density and viscosity differences between the fluid phases could not entirely explain the droplet migration to vortex cores. It was hypothesized that interfacial tension is an important factor for the formation of the banded structure.

The effect of interfacial surface tension on stratified two-phase Couette flow has been a subject of several reports. In a study of unbounded two-fluid Couette flow, Hooper and Boyd (1983) demonstrated that in the absence of surface tension the interface between the two fluids is always unstable to short wavelength perturbations. Joseph et al. (1985) performed a stability analysis of the cylindrical interface between a centrifugally stratified pair of immiscible fluids in the absence of gravity and showed that stability is determined by a dimensionless group, J, that has a definition similar to the Weber number:

$$J = \frac{(\rho_2 - \rho_1)\Omega_i^2 r_i^3}{\sigma}, \qquad (1)$$

where ρ_1 and ρ_2 are the densities of the two fluids, r_i and Ω_i are the inner cylinder radius and angular velocity, and σ is the interfacial surface tension. In particular, global stability occurs when $J > 4$. In a similar numerical study of stratified two-phase flow between corotating cylinders, Renardy and Joseph (1985) extended the analysis by computationally exploring the stability of the interface for various combinations of relative fluid viscosities and configurations.

In this article we report the results of experiments and numerical simulations designed to elucidate the origin of banded flow patterns in emulsified two-phase Taylor-Couette-Poiseuille flow with a fixed outer cylinder (and for low disperse-phase volume fractions so that phase inversion is not possible). In particular, we demonstrate that the banded flow pattern is driven by centrifugal forces within the vortices, and we develop a scaling relation that describes conditions leading to banded flows.

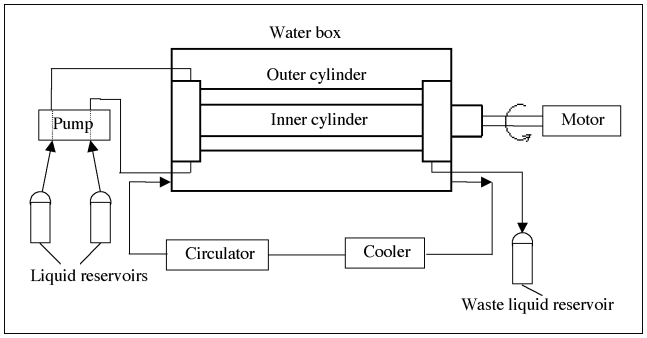

Figure 1. Taylor-Couette cell and associated apparatus.

Experimental Procedure

The experimental setup is shown in Figure 1. The flow cell is arranged horizontally along its main axis and consists of a stainless-steel inner cylinder and a Lucite outer cylinder. The entire assembly is surrounded by a transparent Lucite box, which contains a circulating constant temperature water–ethylene glycol bath. The outer cylinder is fixed and the inner cylinder is driven by a compumotor control system (CMA, Minneapolis, MN). A double-piston pump (Eldex Laboratories, Inc.) was used to supply two separate degassed feed streams to the flow cell. One feed consisted of kerosene dyed red with Oil Red O, and the other feed was deionized water. Physical specifications and operating parameters for the Couette cell are listed in Table 2.

The distribution of kerosene in the column was monitored using a color video camera and recorded through a VCR for subsequent image analysis. In each experiment, the gap was initially filled with water and the inner cylinder was accelerated from rest to the desired angular velocity at an angular acceleration of 6.3 rad/s^2. Upon reaching the desired speed, the inlet pump was started and image collection was begun. The vortex structure was allowed to reach steady state (approximately one hour or three residence times) and photographs of the column were taken using a 35-mm camera

Table 2. Physical and Operating Parameters of the Couette Cell Used in Experiments

Physical Specifications		Operating Parameters	
r_i	1.11 cm	T	20°C
r_o	1.27 cm	Ω_i	31.4–314 rad/s
D	0.32 cm	α_f	0.01–0.4
L	23.5 cm	Re_z	0.41–0.86
σ	0.3 ~ 25 dyne/cm	Re_θ	300–5,000
ρ_{water}	0.9982 g/cm^3		
$\rho_{kerosene}$	0.786 g/cm^3		
μ_{water}	1.005 cp (mPa·s)		
$\mu_{kerosene}$	3.0 cp (mPa·s)		

equipped with a 50-mm macro lens and polarizing filter. All pictures were taken from the same location using ASA 400 film at a shutter speed of 1/1000 second and aperture of f2.8.

Interfacial tension between the dyed kerosene and water phases was measured using a surface tensiomat (Fisher Scientific Company). In the absence of surfactant, this value was found to be 25.0 dynes/cm at 20°C. Experiments were also performed using detergent (U.S. Patent 05415814) as a surfactant, which was added to deionized water at a concentration of 1 g/L. The surfactant reduced the interfacial surface tension between the kerosene and water by nearly two orders of magnitude (0.3 dynes/cm). Since only catalytic amounts of surfactant will reduce surface tension, all surfactant-free experiments were performed before experiments that employed surfactant. However, it should be noted that experiments without surfactant were repeatable even after performing experiments with surfactant, provided that the apparatus was first dismantled and thoroughly cleaned to remove residual surfactant.

Mechanism of Banded Flow

Figure 2 shows photographs of the Couette cell for two experiments performed under identical conditions but with different interfacial surface tension. The resulting flow patterns and dispersed-phase drop sizes are quite different. Figure 2a exhibits a typical banded structure obtained in the absence of surfactant and consisting of vortex cores populated with relatively large dyed kerosene droplets. In contrast, Figure 2b shows that the introduction of surfactant leads to a fine, apparently homogeneous emulsion.

The effect of surface tension on the mean droplet diameter, d_p, can be calculated from the correlation developed by Haas (1987) for liquid dispersions undergoing turbulent Couette flow:

$$\frac{d_p}{D} = 150 We^{-0.65} Re_\theta^{-0.2} \left(\frac{\mu_p (r_o - r_i)}{\mu_c r_i} \right)^{1/2}, \qquad (2)$$

where D is the hydraulic diameter of the Couette cell (twice the gapwidth), r_o is the inner radius of the outer cylinder, and μ_p and μ_c are the disperse and continuous-phase viscosities. The Weber and azimuthal Reynolds numbers used in the preceding correlation are defined by $We = (D\Omega_i^2 r_i^2 \rho_c)/\sigma$ and $Re_\theta = (D\Omega_i r_i \rho_c)/2\mu_c$. The mean droplet diameters predicted by Eq. 2 corresponding to the conditions used to obtain the images in Figures 2a and 2b are 4.1×10^{-2} cm and 2.1×10^{-3} cm, respectively. Careful inspection of Figure 2a reveals that droplet diameters are approximately one-quarter the gapwidth, which is in reasonable agreement with the value predicted by Haas's correlation. Individual droplets cannot be discerned in Figure 2b, but the 20-fold decrease in droplet diameter predicted by Haas's correlation is not inconsistent with the image.

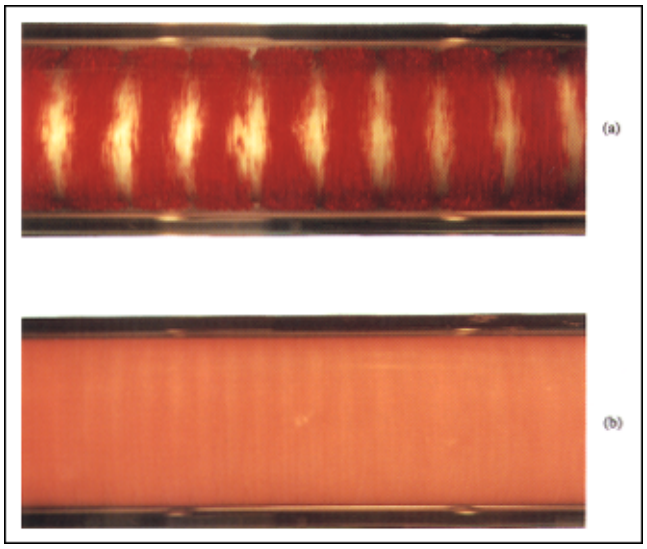

Figure 2. Flow pattern and drop size: with vs. without surfactant for $\alpha_f = 0.1$, $\Omega_i = 314$ s^{-1}, $Re_z = 0.62$.

(a) $\sigma = 25$ dyne/cm; (b) $\sigma = 0.3$ dyne/cm. Only a few vortices in the central part of the column are shown.

The change from the banded flow pattern at high surface tension to a spatially homogeneous emulsion at low surface tension suggests the following interpretation. When the surface tension is high (large droplets), the centrifugal forces arising from the rotation of the Taylor vortices (around an axis passing through their cores) cause the less dense disperse-phase droplets to migrate to vortex cores. When the interfacial surface tension is very low, the droplets are sufficiently small so that they closely follow the movement of the surrounding fluid; the centrifugal force acting on the droplets is not strong enough to overcome turbulent fluctuations that disperse the droplets homogeneously in the gap.

Assuming that the preceding mechanism correctly accounts for the banded flow pattern, a criterion that estimates the transition between banded and homogeneous flow patterns can be obtained by comparing the characteristic time for a droplet (with density $\rho_p < \rho_c$) released on the outer edge of a Taylor vortex to migrate to the core due to centrifugal forces, τ_c, with the characteristic time scale for a droplet to move from the vortex core to the vortex periphery due to turbulent diffusion, τ_t. Consider a steady-state radial force balance on a droplet with diameter d_p released at the edge of a Taylor vortex:

$$\frac{\pi}{6} d_p^3 (\rho_c - \rho_p) \frac{u_\theta^2}{r} = 3\pi \mu_c d_p u_r. \qquad (3)$$

The left side of the equation represents "centrifugal buoyancy," which is balanced by drag forces, which are assumed to be Stokesian. It should be noted that the droplet radial and azimuthal velocities, u_r and u_θ, as well as the coordinate r appearing in Eq. 3, are taken with respect to the rotational axis of the vortex, rather than the main axis of the inner cylinder. Furthermore, we have assumed that the continuous-phase fluid has no radial velocity component with respect to the rotational axis of the vortex, and we neglect droplet interactions, such as coalescence and breakup. The characteristic time for migration from the vortex periphery to the core can be estimated from u_r just defined:

$$\tau_c = \frac{9\mu_c}{8(\rho_c - \rho_p)u_\theta^2}\left(\frac{D}{d_p}\right)^2. \tag{4}$$

The characteristic time scale for transport of droplets from vortex cores to vortex outer layers can be estimated from the turbulent eddy diffusivity so that

$$\tau_t = \frac{D^2\rho_c}{16\mu_t}, \tag{5}$$

and where μ_t is the turbulent viscosity. The ratio of Eqs. 4 and 5 yields:

$$\frac{\tau_c}{\tau_t} = \frac{18\mu_c\mu_t}{(\rho_c - \rho_p)\rho_c d_p^2 u_\theta^2}, \tag{6}$$

which should have a value of order unity near the transition between the banded and homogeneously dispersed states. Note that Eq. 6 depends upon both the physical dimensions of the Couette cell and the operating parameters indirectly through d_p, u_θ, and μ_t. Also, the analysis leading to Eq. 6 is identical for a solid or liquid disperse phase.

Numerical Simulations

In order to numerically explore the applicability of Eq. 6 for predicting the distribution of a disperse phase with $\rho_p < \rho_c$ undergoing turbulent Taylor-Couette flow, axisymmetric simulations were performed using the computational fluid dynamics software FLUENT (Version 5). The multiphase flow was modeled using FLUENT's implementation of the algebraic slip mixture (ASM) model using an approach described in Manninen et al. (1996), which can provide results comparable to a full two-phase model (particularly when the interaction of the phases is not well described), but with far less computational effort. The central feature of the ASM model is that rather than solving separate equations of continuity and momentum for each phase, a single momentum equation for the mixture is solved simultaneously with the equations of continuity for the mixture and for the disperse phase. In addition, the relative (slip) velocity between the disperse phase and the continuous phase is provided by an algebraic expression obtained from a force balance applied to a disperse-phase particle. Turbulence is simulated by applying the Reynolds stress model to the mixture. A number of assumptions associated with the ASM model are employed, including (1) particles are taken to be spherical, (2) the disperse-phase particles have uniform and constant diameter, (3) no mass transfer is allowed between phases, (4) interfacial forces can be neglected, (5) virtual mass and Basset terms can be neglected, and (6) the individual phase pressures are taken to be equal. Several other approximations are described more fully by Manninen et al. (1996). The resulting model equations can be expressed as:

$$\frac{\partial\rho_m}{\partial t} + \nabla\cdot(\rho_m\boldsymbol{u}_m) = 0 \tag{7}$$

$$\frac{\partial}{\partial t}(\rho_m\boldsymbol{u}_m) + \nabla\cdot(\rho_m\boldsymbol{u}_m\boldsymbol{u}_m) = -\nabla p_m - \nabla\cdot\left[\rho_m w(1-w)\boldsymbol{u}_{cp}\boldsymbol{u}_{cp}\right] + \nabla\cdot(\tau_{Gm}) + \rho_m\boldsymbol{g} \tag{8}$$

$$\frac{\partial\alpha}{\partial t} + \nabla\cdot\alpha\boldsymbol{u}_m = -\nabla\cdot\left[\alpha(1-w)\boldsymbol{u}_{cp}\right], \tag{9}$$

where α and w are the disperse-phase volume and mass fractions, respectively. The slip velocity, $\boldsymbol{u}_{cp}$, is obtained from the force balance:

$$|\boldsymbol{u}_{cp}|\boldsymbol{u}_{cp} = \frac{4d_p(\rho_p - \rho_m)}{3C_D\rho_c}\left[\boldsymbol{g} - (\boldsymbol{u}_m\cdot\nabla)\boldsymbol{u}_m - \frac{\partial\boldsymbol{u}_m}{\partial t}\right], \tag{10}$$

and the generalized stress tensor is given by

$$\tau_{Gm} = (\mu_m + \mu_{Tm})\left[\nabla\boldsymbol{u}_m + (\nabla\boldsymbol{u}_m)_T\right] - \frac{2}{3}\rho_m k_m\boldsymbol{I}. \tag{11}$$

In addition, FLUENT employs the following expression for the drag coefficient due to Schiller and Nauman (see Clift et al., 1978):

$$\begin{aligned} C_D &= \frac{24}{Re_p}\left(1 + 0.15Re_p^{0.687}\right) && Re_p < 1{,}000 \\ &= 0.44 && Re_p > 1{,}000, \end{aligned} \tag{12}$$

where Re_p is the particle Reynolds number. Notice that Eqs. 10 and 12 reduce to Eq. 3 for a steady azimuthal Stokesian flow with negligible gravitational effects.

The physical specifications of the Couette cell and the fluids (kerosene and water) used in the experiments were also used in the simulations. As was expected, streamfunction plots revealed a mean flow reminiscent of laminar Taylor vortex flow. Vortex axial wavelengths calculated from the simulations were compared to corresponding experimental data, and agreement was found within a precision of approximately 3.5%, thereby providing further evidence for the validity of the ASM model simulations. Simulations using both the full reactor length (23.6 cm) and a shorter length (1.6 cm) also revealed that the reactor length did not affect the spatial distribution of the disperse phase within the Taylor vortices. Hence, most simulations were performed using the shorter reactor length. Calculations were also performed using vari-

ous grid resolutions, but no significant differences in the mean flow were found for grid spacing smaller than 5.3×10^{-3} cm, which corresponds to 30×300 grid points in the radial and axial directions, respectively. Each simulation was continued until steady-state mean velocity fields and volume fraction distributions developed and all convergence criteria were satisfied.

Simulation Results

Figure 3 illustrates stream-function plots and disperse-phase volume-fraction distributions for operational parameters and drop sizes corresponding to the experiments depicted in Figure 2. Using the larger drop size predicted by Eq. 2 in the absence of surfactant, a strongly banded structure is produced in which there is a large enrichment of kerosene in the vortex cores (Figure 3b), in agreement with the image obtained from experiment in Figure 2a. Similarly, the simulation predictions of a spatially homogeneous dispersion of kerosene in Figure 3d agree with the corresponding experiments in Figure 2b for the case in which surfactant was used.

In order to determine if the dimensionless quantity defined by Eq. 6 correctly describes the competition between centrifugal forces and turbulent diffusion that determines whether or not the flow pattern is banded, numerous simulations were performed using various combinations of operating parameters (such as inner cylinder rotation rate, organic-phase feed volume fraction), as well as different disperse-phase droplet diameters. It should be noted that for liquid–liquid systems, the independent manipulation of droplet diameter can be accomplished by continuously varying the interfacial surface tension. For a solid disperse phase, the particle diameters can obviously be chosen arbitrarily.

In order to calculate the dimensionless ratio of centrifugal and turbulent time scales in Eq. 6, the azimuthal velocity (u_θ, with respect to the vortex rotational axis) on the outer edge of a Taylor vortex must be determined. This quantity can easily be estimated from the FLUENT simulations by equating u_θ to the mean radial fluid velocity (with respect to the inner cylinder rotational axis) at a vortex inflow or outflow boundary. The turbulent viscosity in the vortex core, μ_t, also appears in Eq. 6, and this quantity is also calculated in the FLUENT simulations.

In order to quantify the extent to which a flow is banded, we have calculated the ratio of the disperse-phase volume fractions in the vortex core and in the reactor feed, α_c/α_f. Figure 4 shows the relationship between this vortex-core volume-fraction enhancement as a function of the time-scale ratio τ_c/τ_t and by using various inner cylinder speeds, droplet sizes, fluid compositions, and axial flow rates. As was expected, the data appear to lie on a universal curve such that α_c/α_f rapidly decreases to an asymptotic value of unity as the ratio τ_c/τ_t is increased from zero to one. The interpretation of this result is clear: the banded flow pattern is caused by centrifugal forces acting on the less dense droplet phase and overcoming the dispersive turbulent transport.

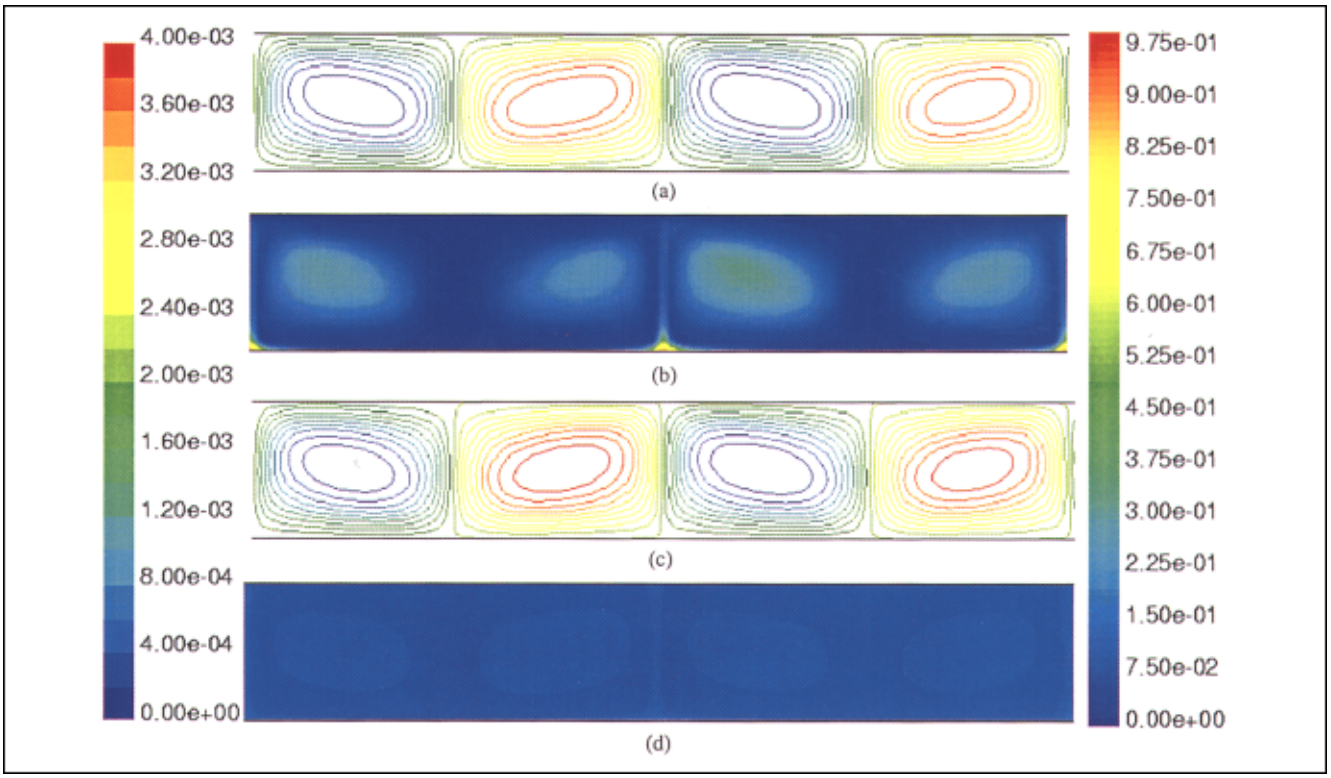

Figure 3. FLUENT predictions for vortex streamlines and kerosene volume fraction for conditions corresponding to Figure 2.

(a) and (b) correspond to Figures 2a and 2b, and (c) and (d) correspond to conditions of Figure 2b.

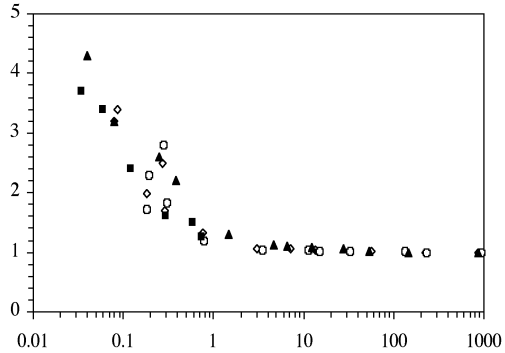

Figure 4. Disperse phase core volume fraction enhancement: α_c/α_f, vs. τ_c/τ_t for various conditions: ■ ($\alpha_f = 0.1$, $Re_\theta = 4{,}830$, $Re_z = 0.62$), ○ ($\alpha_f = 0.1$, $Re_\theta = 2{,}900$, $Re_z = 0.62$), ▲ ($\alpha_f = 0.1$, $Re_\theta = 4830$, $Re_z = 4.1$), △ ($\alpha_f = 0.2$, $Re_\theta = 762$, $Re_z = 0.86$).

Disperse-phase particle diameters varied in the range 5.5×10^{-5} cm $- 3.7\times 10^{-2}$ cm.

The photographs in Figures 5a–5d provide further, albeit qualitative, evidence for the validity of Eq. 6 as an index for predicting the "bandedness" of the flow. The experiments that produced these images were carried out with a constant interfacial surface tension ($\sigma = 0.3$ dynes/cm), axial flow rate ($Re_z = 0.62$), and kerosene volume fraction ($\alpha_f = 0.1$), but with different inner cylinder angular velocities ranging from approximately 30 rad/s to 190 rad/s. It is clearly evident that the dispersed kerosene droplets become increasingly homogeneously distributed in the annulus as the inner cylinder speed increases. Calculation of the ratios τ_c/τ_t corresponding to Figures 5b–5d (making use of Haas's correlation, Eq. 2, and FLUENT simulation results) yields $\tau_c/\tau_t = 0.06$ ($\Omega_i =$ 62.8 rad/s), 0.58 ($\Omega_i = 126$ rad/s), and 0.74 ($\Omega_i = 188$ rad/s). The corresponding core volume-fraction enhancement factors are $\alpha_c/\alpha_f = 3.4$, 1.5, and 1.2, respectively, and these are consistent with the trend shown in Figure 5.

Single-Phase Behavior

The low surface-tension experiments pictured in Figure 5 also reveal behavior previously unreported for liquid–liquid Taylor-Couette flow. Specifically, the vortices in Figure 5a are wavy. At a higher inner cylinder angular velocity, (Fig. 5b), the waves appear to be modulated. Upon further increasing the inner cylinder speed, as in Figures 5c and 5d, the waves disappear, probably indicating the onset of turbulent Taylor vortex flow. For single-phase flow and the particular geometry used in our experiments, the azimuthal Reynolds number ratios ($Re_\theta/Re_{\theta,c}$) for the transitions to wavy, modulated wavy, and turbulent Taylor vortex flow are given by 1.7, 8.5, and 11.8, respectively (Tam and Swinney, 1987; Andereck et al., 1986). Here, $Re_{\theta,c}$ represents the critical azimuthal Reynolds number for the onset of laminar Taylor vortex flow. Using volume-weighted average kinematic viscosities, the azimuthal Reynolds number ratios corresponding to the images in Figures 5a–5d are 3.8, 7.7, 15, and 23, respectively. Although we have not precisely determined

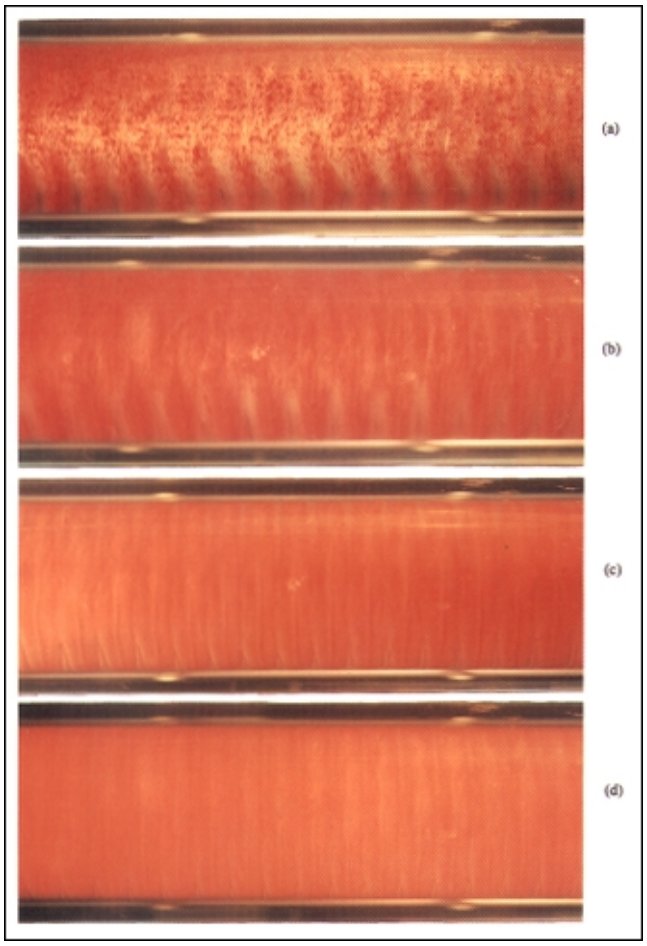

Figure 5. Images showing the effect of increasing Re_θ for fixed $\alpha_f = 0.1$, $Re_z = 0.62$, $\sigma = 0.3$ dyne/cm, and where $Re_\theta/Re_{\theta,c}$ = (a) 3.8; (b) 7.7; (c) 15.0; (d) 23.0.

the Reynolds number ratios at the transitions between the various flow patterns, Figure 5 does not exclude the possibility that they may be identical to the known values for the single-phase case, provided that mixture properties are used in the calculations.

Disperse-Phase Density

Thus far we have considered the origin of the banded structure when the less dense phase (kerosene) is dispersed in water. However, Campero and Vigil (1999) reported observing banded structures for the case in which water was dispersed in kerosene, and such bands cannot be explained by centrifugally driven droplet migration to vortex cores. Indeed, when the disperse-phase density is greater than the continuous-phase density, the centrifugal forces within a vortex would be expected to force droplets to the vortex periphery. However, it may be possible that the heavier droplet phase distributes preferentially at inflow or outflow boundaries between vortices, thereby producing a banded appearance. Indeed, FLUENT simulations using the heavier water

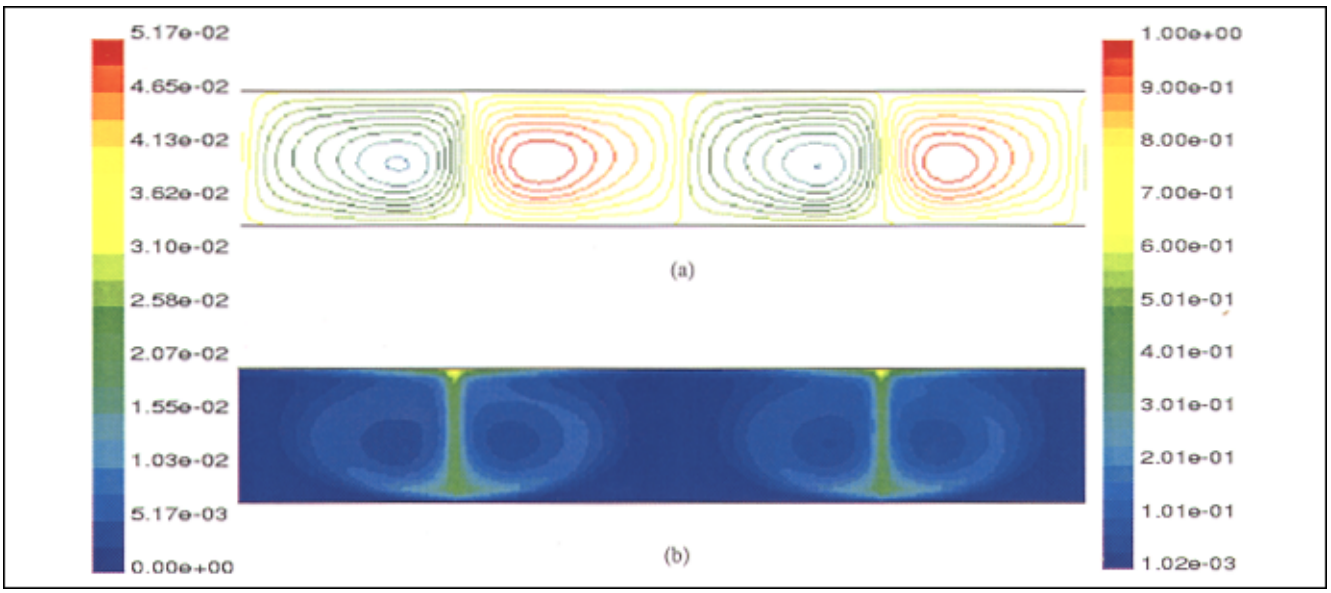

Figure 6. FLUENT predictions: (a) vortex streamlines; (b) water-volume fraction for an emulsion of water (10% by volume) dispersed in kerosene (90%).

Other operational parameters are given by $Re_\theta = 5815, Re_z = 9.6$, and $\sigma = 25$ dyne/cm.

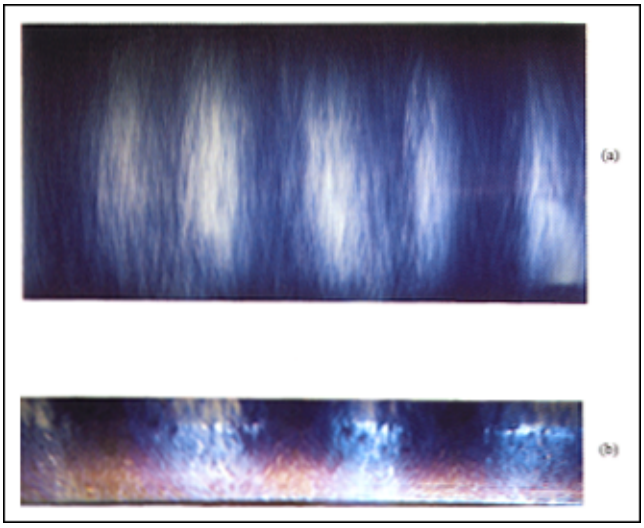

Figure 7. Images from an experiment corresponding to the conditions in Figure 6, with water dyed blue and kerosene undyed.

A wide-angle view of the central portion of the reactor is shown in (a). A closeup image of part of the annular gap is shown in (b).

as the disperse phase predict droplet accumulation at inflow boundaries, as shown in Figure 6. Photographs from corresponding experiments (Figure 7) show that the flow is indeed banded, but it is impossible to determine from these images whether the dyed water phase resides at inflow boundaries or in the vortex core.

Discussion

Banded distributions of disperse-phase droplets are characteristic of liquid–liquid Taylor-Couette flow with a fixed outer cylinder. These structures arise when centrifugal forces associated with the rotation of the vortices themselves, as opposed to the inner cylinder, are sufficiently strong to cause droplet migration to vortex cores ($\rho_p < \rho_c$) or to vortex inflow boundaries ($\rho_p > \rho_c$). For the case of a less dense disperse phase, the scaling relation provided by Eq. 6 appears to correctly predict the "bandedness" of liquid–liquid Taylor-Couette flow. However, its usefulness as a predictive tool is limited by the lack of prior knowledge concerning (1) the azimuthal velocity component (u_θ, with respect to the vortex rotational axis in the core) on the outer layer of a vortex, and (2) the turbulent viscosity in the vortex cores. Droplet diameters can be estimated by using Haas's correlation, Eq. 2.

As a first approximation, for small particle loadings one would expect u_θ to be independent of α and d_p and to be proportional to the inner cylinder angular velocity so that $u_\theta/\Omega_i r_i = \text{constant}$. Indeed, a plot of this ratio against azimuthal Reynolds number (Figure 8) shows that

$$\frac{u_\theta}{\Omega_i r_i} \cong 0.14. \tag{13}$$

Calculation of the mixture turbulent viscosity at the vortex core is more difficult, as this quantity depends upon the local turbulent kinetic energy and turbulent dissipation, which in turn are composition-dependent quantities.

Equation 6 is strongly dependent on the mean droplet diameter, which in turn depends more sensitively on *We* than on Re_θ, according to Eq. 2. A decrease in interfacial surface tension through the introduction of a surfactant, therefore, is a more effective means for reducing droplet size than is a proportional increase in the angular velocity of the inner cylinder. For fixed interfacial surface tension, experiments and FLUENT simulations show that the disperse phase be-

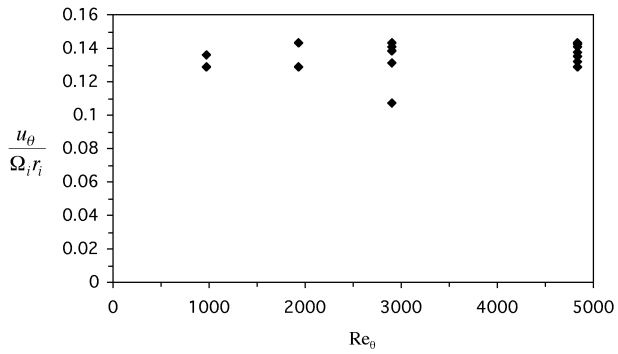

Figure 8. Reduced angular velocity of vortex outer layer (with respect to the vortex rotational axis in the core) vs. azimuthal Reynolds number for $\alpha_f = 0.1$ and disperse-phase particle diameters varying in the range 5.5×10^{-5} cm to 3.7×10^{-2} cm.

comes progressively more homogeneously distributed as the azimuthal Reynolds number is increased.

Acknowledgment

The authors would like to thank Professor Rodney O. Fox at Iowa State University for helpful discussions.

Notation

C_D = drag coefficient, dimensionless
D = hydraulic diameter, = twice the annular gapwidth, cm
d_p = average drop diameter, cm
$\boldsymbol{g}$ = gravitational acceleration vector, m/s^2
k = turbulent kinetic energy, m^2/s^2
L = Couette cell length, cm
p = pressure, kg/s^2
Re_p = particle Reynolds number, $= d_p \rho_c |\boldsymbol{u}_{cp}|/\mu_c$
Re_θ = azimuthal Reynolds number, $= \rho \Omega_i r_i D/2\mu$
Re_z = axial Reynolds number, $= \rho V_z D/\mu$
r_i = outside radius of the inner cylinder, cm
r_o = inside radius of the outer cylinder, cm
T = operating temperature, °C
t = time, s
$\boldsymbol{u}_{cp}$ = slip velocity, $= \boldsymbol{u}_p - \boldsymbol{u}_c$, cm/s
$\boldsymbol{u}_m$ = mixture velocity, $= w\boldsymbol{u}_p + (1-w)\,\boldsymbol{u}_c$, cm/s
u_θ = droplet azimuthal velocity with respect to the vortex rotational axis passing through the vortex core, cm/s
u_r = droplet radial velocity with respect to the vortex rotational axis passing through the vortex core, cm/s
V_z = average axial velocity, cm/s
w = disperse phase mass fraction, dimensionless
We = Weber number, $= \rho\,(\Omega_i r_i)^2 D/\sigma$

Greek letters

α = disperse phase volume fraction, dimensionless
Γ = aspect ratio, $= 2L/D$
μ_t = turbulent viscosity, kg/m·s
μ = fluid molecular viscosity, kg/m·s
ρ = fluid density, g/cm^3
σ = interfacial tension, dyne/cm
τ_{Gm} = generalized stress tensor, kg/m·s^2
τ_c = characteristic time for a droplet to migrate to a vortex core due to centrifugal forces, s
τ_t = characteristic time for a droplet to migrate from a vortex core due to turbulent dispersion, s
Ω_i = rotation rate of the inner cylinder, rad/s

Subscripts

c = continuous phase
p = particulate phase
f = feed condition
m = mixture property or variable
T = turbulent

Literature Cited

Albert, F., and F. Charru, "Small Reynolds Number Instability in Two-Layer Couette Flow," *Eur. J. Mech. B — Fluids*, **19**, 229 (2000).
Ameer, G. A., E. A. Grovender, B. Obradovic, C. L. Cooney, and R. Langer, "RTD Analysis of a Novel Taylor-Couette Flow Device for Blood Detoxification," *AIChE J.*, **45**, 633 (1999).
Andereck, C. D., S. S. Liu, and H. L. Swinner, "Flow Regimes in a Circular Couette System with Independently Rotating Cylinders," *J. Fluid Mech.*, **164**, 155 (1986).
Baier, G., and M. D. Graham, "Two-Fluid Taylor-Couette Flow: Experiments and Linear Theory for Immiscible Liquids Between Corotating Cylinders," *Phys. Fluids*, **10**, 3045 (1998).
Baier, G., and M. D. Graham, "Two-Fluid Taylor-Couette Flow With Countercurrent Axial Flow: Linear Theory for Immiscible Liquids Between Corotating Cylinders," *Phys. Fluids*, **12**, 294 (2000).
Bernstein, G. J., D. E. Grosvenor, J. F. Lenc, and N. M. Levitz, "A High-Capacity Annular Centrifugal Contactor," *Nucl. Technol.*, **20**, 200 (1973).
Campero, R. J., and R. D. Vigil, "Axial Dispersion During Low Reynolds Number Taylor-Couette Flow: Intra-Vortex Mixing Effects," *Chem. Eng. Sci.,* **52**, 3303 (1997a).
Campero, R. J., and R. D. Vigil, "Spatiotemporal Patterns in Liquid-Liquid Taylor-Couette-Poiseuille Flow," *Phys. Rev. Lett.*, **79**, 3897 (1997b).
Campero, R. J., and R. D. Vigil, "Flow Patterns in Liquid–Liquid Taylor-Couette-Poiseuille Flow," *Ind. Eng. Chem. Res.*, **38**, 1094 (1999).
Caton, F., B. Janiaud, and E. J. Hopfinger, "Stability and Bifurcations in Stratified Taylor-Couette Flow," *J. Fluid Mech.,* **419**, 93 (2000).
Charru, F., and E. J. Hinch, "Phase Diagram of Interfacial Instabilities in a Two-Layer Couette Flow and Mechanism of the Long-Wave Instability," *J. Fluid Mech.*, **414**, 195 (2000).
Clift, R., J. R. Grace, and M. E. Weber, *Bubbles, Drops, and Particles*, Academic Press, London, p. 351 (1978).
Cohen, S., and D. M. Maron, "Experimental and Theoretical Study of a Rotating Annular Flow Reactor," *Chem. Eng. J.*, **27**, 87 (1983).
Cohen, S., and D. M. Maron, "Analysis of a Rotating Annular Reactor in the Vortex Flow Regime," *Chem. Eng. Sci.*. **46**, 123 (1991).
Davis, M. W., and E. J. Weber, "Liquid-Liquid Extraction Between Rotating Concentric Cylinders," *Ind. Eng. Chem.*, **52**, 929 (1960).
Desmet, G., H. Verelst, and G. V. Baron, "Transient and Stationary Axial Dispersion in Vortex Array Flows—II. Decoupling of Inter- and Intra-Vortex Transport Phenomena," *Chem. Eng. Sci.*, **52**, 2403 (1997a).
Desmet, G., H. Verelst, and G. V. Baron, "Transient and Stationary Axial Dispersion in Vortex Array Flows—I. Axial Scan Measurements and Modeling of Transient Dispersion Effects," *Chem. Eng. Sci.*, **52**, 2383 (1997b).
Haas, P. A., "Turbulent Dispersion of Aqueous Drops in Organic Liquids," *AIChE J.*, **33**, 987 (1987).
Hooper, A. P., and W. G. C. Boyd, "Shear-Flow Instability at the Interface Between Two Viscous Fluids," *J. Fluid Mech.*, **128**, 507 (1983).
Holeschovsky, U. B., and C. L. Cooney, "Quantitative Description of Ultrafiltration in a Rotating Filtration Device," *AIChE J.*, **37**, 1219 (1991).
Holl, R. A., "Methods and Apparatus for High-Shear Material Treatment," U.S. Patent No. 5,538,191 (1996).
Imamura, T., K. Saito, and S. Ishikura, "A New Approach to Continuous Emulsion Polymerization," *Poly. Int.*, **30**, 203 (1993).
Joseph, D. D., P. Singh, and K. Chen, "Couette Flows, Rollers, Emulsions, Tall Taylor Cells, Phase Separation and Inversion, and a Chaotic Bubble in Taylor-Couette Flow of Two Immiscible Liquids," *Nonlinear Evolution of Spatio-Temporal Structures in Dissipative Continuous Systems,* Plenum Press, New York, p. 169 (1990).

Joseph, D. D., K. Nguyen, and G. S. Beavers, "Non-Uniqueness and Stability of the Configuration of Flow of Immiscible Fluids with Different Viscosities," *J. Fluid Mech.*, **141**, 319 (1984).
Joseph, D. D., Y. Renardy, M. Renardy, and K. Nguyen, "Stability of Rigid Motions and Rollers in Bicomponent Flows of Immiscible Liquids," *J. Fluid Mech.*, **153**, 151 (1985).
Joseph, D. D., and L. Preziosi, "Stability of Rigid Motions and Coating Films in Bicomponent Flows of Immiscible Liquids," *J. Fluid Mech.*, **185**, 323 (1987).
Jung, W. M., S. H. Kang, W.-S. Kim, and C. K. Choi, "Particle Morphology of Calcium Carbonate Precipitated by Gas-Liquid Reaction in a Couette-Taylor Reactor," *Chem. Eng. Sci.*, **55**, 733 (2000).
Kataoka, K., H. Doi, T. Hongo, and M. Futagawa, "Ideal Plug-Flow Properties of Taylor Vortex Flow," *J. Chem. Eng. Jpn.*, **8**, 472 (1975).
Kataoka, K., N. Ohmura, M. Kouzu, Y. Simamura, and M. Okubo, "Emulsion Polymerization of Styrene in a Continuous Taylor Vortex Flow Reactor," *Chem. Eng. Sci.*, **50**, 1409 (1995).
King, M. R., D. T. Leighton, Jr., and M. J. McCready, "Stability of Oscillatory Two-Phase Couette Flow: Theory and Experiment," *Phys. Fluids*, **11**, 833 (1998).
Leonard, R. A., G. J. Bernstein, R. H. Pelto, and A. A. Ziegler, "Liquid-Liquid Dispersion in Turbulent Couette Flow," *AIChE J.*, **27**, 495 (1981).
Manninen, M., V. Taivassalo, and S. Kallio, "On the Mixture Model for Multiphase Flow," VTT Publications, Technical Research Center of Finland (1996).
Miller, R. L., A. G. Fredrichson, A. H. Brown, and H. M. Tsuchiya, "Hydromechanical Method to Increase Efficiency of Algal Photosynthesis," *Ind. Eng. Chem. Process Des. Dev.,* **3**, 134 (1964).
Ogihara, T., G. Matsuda, T. Yanagawa, N. Ogata, K. Fujita, and M. Nomura, "Continuous Synthesis of Monodispersed Silica Particles Using Couette-Taylor Vortex Flow," *J. Ceram. Soc. Jpn., Int.*, **103**, 151 (1995).
Ouyang, Q., H. L. Swinney, J. C. Roux, P. De Kepper, and J. Boissonade, "Recovery of Short-Lived Chemical Species in a Couette Flow Reactor," *AIChE J.*, **38**, 502 (1992).
Renardy, Y., and D. D. Joseph, "Couette Flow of Two Fluids Between Concentric Cylinders," *J. Fluid Mech.*, **150**, 381 (1985).
Roberts, R. M., Y. Ye, E. A. Demekhin, and H. C. Chang, "Wave Dynamics in Two-Layer Couette Flow," *Chem. Eng. Sci.*, **55**, 345 (2000).
Schneyer, G. P., and S. A. Berger, "Linear Stability of the Dissipative, Two-Fluid, Cylindrical Couette Problem. Part 1. The Stably-Stratified Hydrodynamic Problem," *J. Fluid Mech.*, **45**, 91 (1971).
Sczechowski, J. G., C. A. Koval, and R. D. Noble, "A Taylor Vortex Reactor for Heterogeneous Photocatalysis," *Chem. Eng. Sci.*, **50**, 3163 (1995).
Tam, W. Y., and H. L. Swinney, "Mass Transport in Turbulent Couette-Taylor Flow," *Phys. Rev. A*, **36**, 1374 (1987).
Thornton, J. D., and H. R. C. Pratt, "Liquid-Liquid Extraction: Part VII. Flooding Rates and Mass Transfer Data for Rotary Annular Columns," *Trans. Inst. Chem. Eng.*, **31**, 289 (1953).
Tsao, Y. M. D., E. Boyd, and G. Spaulding, "Fluid Dynamics Within a Rotating Bioreactor in Space and Earth Environments," *J. Spacecr. Rockets*, **31**, 937 (1994).
Vigil, R. D., Q. Ouyang, and H. L. Swinney, "Spatial Variation of a Short-Lived Intermediate Chemical Species in a Couette Reactor," *J. Chem. Phys.*, **96**, 6126 (1992).
Wereley, S. T., and R. M. Lueptow, "Inertial Particle Motion in a Taylor Couette Rotating Filter," *Phys. Fluids*, **11**, 325 (1999).
Wronski, S., E. Dluska, R. Hubacz, and E. Molga, "Mass Transfer in Gas-Liquid Couette-Taylor Flow in a Membrane Reactor," *Chem. Eng. Sci.*, **54**, 2963 (1999).
Zhu, X.-Y., R. J. Campero, and R. D. Vigil, "Axial Mass Transport in Liquid-Liquid Taylor-Couette-Poiseuille Flow," *Chem. Eng. Sci.*, **55**, 5079 (2000).

Manuscript received Jan. 2, 2001, and revision received Apr. 25, 2001.